Chemical Engineering Journal 103 (2004) 99–113

Chemical Engineering Journal

www.elsevier.com/locate/cej

The conceptual design of a PEMFC system via simulation

S.K. Kamarudin*, W.R.W. Daud, A.Md. Som, A.W. Mohammad, S. Takriff, M.S. Masdar

Department of Chemical and Process Engineering, National University of Malaysia, 43600 UKM Bangi, Selangor, Malaysia

Received 3 January 2004; received in revised form 20 May 2004; accepted 1 June 2004

Abstract

The main objective of this study is to introduce the short cut design method for the conceptual design of a proton electrolyte of membrane fuel cell (PEMFC) system. Initially, as a model development of the system, this paper tends to focus on the overall system design of the fuel cell. Basically, the system consist of five major units, namely; Auto-thermal reformer (ATR), water gas shift reactor (WGS), membrane, pressure swing adsorber (PSA) and fuel cell stack. The ATR and WGS are designed based on the rate of reaction and variations in volume. For membrane unit, the expression of the length and surface area are simplified in terms of NTU and HTU. The PSA process is quite complicated and there are many parameters to be decided; therefore, we simplify the design of the PSA by introducing Daud bed utilisation factor. For the stack design, the voltage for single cell, number of cells required, current density, power density and finally the current flow in the stack are determined in this study. The material and heat balance of the system are also presented here. Finally the overall fuel cell efficiency is also determined. System with power output as 5 kW of PEMFC is taken as a case study. Methanol is taken as a primary fuel source to the ATR system, which is fed together with steam and oxygen. The conceptual design indicates that if the mole ratio of O_2/MeOH is 0.20–0.25, then the hydrogen selectivity is around 2.5–2.6 for complete methanol conversion. With that the ratio of MeOH:H_2O and MeOH:O_2 are taken as 1:1.3 and 1:0.25, respectively. The conceptual design also proves that WGS reaction plays a very important role in the reduction of the CO produced in the ATR. In the conceptual design, the ATR product contains H_2: 73%, CO: 2%, and CO_2: 25%. The CO level is then further reduced to less than 2000 ppm in the WGS reactor. Hydrogen-rich reformate, which is produced by reforming primary fuels in the fuel processor system contains significant amount of CO, is further reduced by tubular ceramic membrane (TCM) and a pressure swing adsorber (PSA) in series. From the overall material balance, it is observed that the final concentration of hydrogen is purified to 99.99% with the concentration of CO is reduced to less than 10 ppm before entering the fuel cell stack. Finally this paper will calculate the overall heat balance of the system in order to calculate the power plant efficiency. The gross efficiency of the system is calculated as 49.3% while the net efficiency of the system after considering the parasitic load is estimated as 45.5%.

Keywords: Fuel cell; Conceptual design; Simulation; Fuel processor; Hydrogen purifier unit; Fuel cell stack

1. Introduction

With the aim of obtaining vehicles with the intrinsic possibility of zero emission, new solutions of the problem were examined and tested in the early 1990s. One of the most promising technologies for obtaining the desired result is represented by the fuel cell. Industrial solutions using this electrochemical device in the automotive industry are the proton-exchange membrane fuel cells, producing electrical energy at low working temperature with high efficiency [1–5]. Furthermore, these systems offer the best solution for reducing pollution to zero in city centres. Other advantages of PEMFCs include: (1) the flexibility with respect to power and capacity achievable devices for energy conversion and energy storage, (2) the long lifetime and long service life, (3) the good ecological balance, (4) very low self-discharge, (5) the low power methanol fuel cells for mobile phone in hybrid system with batteries [6–9], and micro-fuel cells are required for hand held PCs in the sub-Watt range [10,11].

Basically, this paper is divided into four sections. The first section of this paper introduces the PEMFC system and the guideline of this paper. The second section will explain the overall system design and present the shortcut design method for each major unit in the system; the auto-thermal reformer (ATR), water gas shift reactor (WGS), tubular ceramic membrane (TCM), pressure swing adsorber (PSA) and fuel cell stack, that can be used as quick, fast and reliable method for initial conceptual design. The following section will present the overall material and heat balances of the system. Finally the last section will determine the PEMFC system efficiency. A power output of 5 kW of PEMFC is taken as case study.

The fuel source used in this system is methanol since methanol is the most promising organic fuels as compared

* Corresponding author.
E-mail address: ctie@vlsi.eng.ukm.my (S.K. Kamarudin).

1385-8947/$ – see front matter © 2004 Elsevier B.V. All rights reserved.
doi:10.1016/j.cej.2004.06.002

Nomenclature

A	cell active area (cm^2)
A_M	surface are of membrane (cm^2)
A_0	pre-exponential factor ($mol(min\, g_{cat}\, kPa^{0.22})^{-1}$)
c	concentration in gas phase (mol/m^3)
c^*	equilibrium concentration (mol/m^3)
C_{H_2,O_2}	molar concentration of H_2/O_2 in electrolyte (mol/m^3)
$C^{ref}_{H_2,O_2}$	molar concentration of H_2/O_2 in electrolyte at standard condition (mol/m^3)
d_p	pore diameter (cm)
D	diffusivity ($m^2\, s^{-1}$)
D_L	axial dispersion
D_p	bed diameter (cm)
D_t	tube diameter (cm)
D^{agg}	gas diffusivity in electrolyte ($m^2\, s^{-1}$)
E_a	activation energy (kJ/mol)
F	Faraday constant (96,487 C) 96,487 A s mol^{-1}
F_A	output flow of component A (mol/min)
F_{A0}	feed flow of component A (mol/min)
F_{MeOH}	feed flow of methanol (mol/min)
ΔG_{ec}	standards Gibbs activation energy (kJ/mol)
H	Henry's law coefficient ($Pa\, m^3\, mol^{-1}$)
HTU	height of heat transfer unit
i	current (A)
i_0	exchanges of current density (A/m^2)
k	mass transfer coefficient
k_1,k_2	rate constant ($mol/kg_{cat}\, s$)
K	permeability ($gmol\, cm/(cm^2\, s\, atm)$)
K_{eq}	rate constant equilibrium ($mol/kg_{cat}\, s$)
Kn	Knudsen number
l_M	membrane thickness (cm)
L	length (cm)
L_b	bed length (cm)
M	molecular weight ($kg\, mol^{-1}$)
n_F	feed flow rate (mol/min)
n_P	permeate flow rate (mol/min)
n_R	retentate flow rate (mol/min)
n_T	number of tube
N	flux ($kmol/m^2\, s$)
NTU	number of heat transfer unit
P	pressure (Pa)
P_{CO}	partial pressure of CO (Pa)
P_{CO_2}	partial pressure of CO_2 (Pa)
P_{H_2}	partial pressure of H_2 (Pa)
P_{H_2O}	partial pressure of water (Pa)
$p^*_{H_2}$, P_{H_2O}	partial pressure for hydrogen at anode (Pa)
P_{O_2}	partial pressure of O_2 (Pa)
$p^*_{O_2}$	partial pressure for oxygen at anode (Pa)
q	concentration in adsorbed phase (mol/L)
Q_F	volumetric flow rate of feed (m^3/min)
r_p	pore radius (mm)
r_{SRM}	steam reforming rate ($mol/kg_{cat}\, s$)
r_{WGS}	reaction rate for WGS reaction ($mol/kg_{cat}\, s$)
R	ideal gas constant ($8.314\, kg\, m^2\, s^{-2}\, mol^{-1}\, K^{-1}$)
R_g	molecule radius (Å)
R^{agg}	radius of electrolyte (m)
Re	Reynolds number
S	specific surface area of electrode ($cm^2\, cm^{-3}$)
Sc	Schmidt number
Sh	Sherwood number
t_{ideal}	ideal time (s)
T	temperature (K)
u	interstitial velocity (cm/s)
V	volume (cm^3)
V_c	voltage of single cell (V)
w	width of gas channel (cm)
x_r	mole fraction for retentate
X_A	conversion of component A
X_{MeOH}	mass fraction of methanol
y_A	mole fraction of component A
y_p	mole fraction for permeate
z	bed length (cm)

Greek letters

α	separation factor
δ	Daud's bed utilisation parameter
δ_l	electrodes thickness on active area (cm)
ε_p	bed porosity
ε	dry voidage on electrodes (cm)
θ	ratio of n_p/n_f
μ	viscosity (m^2/s)
ν	diffusivity volume
ξ	dimensionless length
τ_{kn}	tortuosity
τ	dimensionless time
ρ	gas density (g/m^3)
ϕ_m	potential of membrane (V)
ϕ_s	potential of electrodes (V)
$\Delta\phi_{eq}$	potential different between the electrodes and membrane at equilibrium (V)

Subscripts

a	anode
c	cathode
F	feed
M	methanol
MO	methanol at initial stage
O_2	oxygen

O_20	oxygen at initial stage
R	recycle
S	steam
S0	steam at initial stage
T	tube
V	volume
1,2	components 1 and 2

to hydrogen: high solubility in aqueous, electrolytes, liquid fuel available at low cost, easily handled as well as transported and stored, high theoretical density of energy (6 kWh/kg) and many experts consider methanol as an ideal hydrogen carrier [2,5], Heizel et al. (2003) [9,12–14]. Besides methanol, steam and oxygen (or air) are also used as feed source to produce hydrogen.

2. Overall system design

Fig. 1 shows the schematic diagram of PEMFC system currently proposed for this study. The main electric power generator in the system is the fuel cell stack (that contains the anode, cathode, PEM and cooling plates) as shown in the diagram. The following paragraphs explain the layout in terms of the flows of oxygen (or air), fuel, processed water, exhaust gases and stack coolant.

Beginning at the right-bottom, air passes through an oxygen concentrator unit in order to separate the O_2 from N_2. This stream will split into two main streams. The smaller oxygen (or air) flow is preheated and fed to an ATR reactor. On the other hands, the larger oxygen (or air) that flows to the HUM 1 is humidified and cooled by injecting liquid water prior to being supplied to the cathode inlet of the fuel cell stack.

The fuel flow circuits begin at the fuel tank (methanol). From the tank, it is pumped to the fuel vaporizer where it is heated and vaporized by the hot stream exhaust gas. It is then fed to the ATR where it reacts with the preheated air and superheated steam to yield the raw reformate. The hot reformate is used to superheat the ATR steam feed. It may then be mixed with additional water and fed to WGS reactor. The fuel gas leaving this reactor will pass through the water adsorber unit. The purpose of this unit is to remove the excess water in the stream before entering the membrane units. The flow that leaves the membrane unit is then cooled by lowering the temperature of the inlet oxygen (or air) and subsequently vaporized the feed methanol to ATR before entering the adsorber. Finally the purified hydrogen fuel flow will be humidified to 100% by HUM 2 and will enter the anode side of the stack.

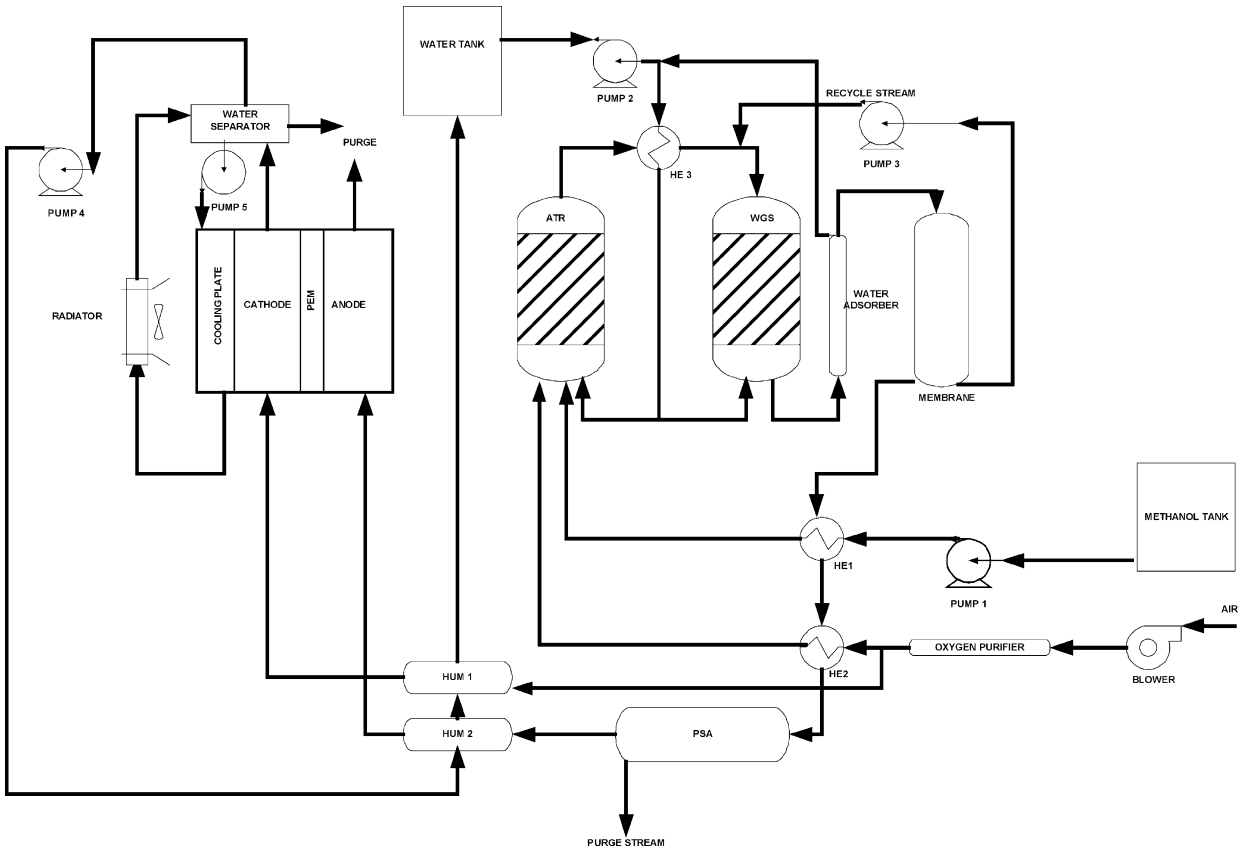

Fig. 1. Schematic diagram of proposed PEMFC system in this study.

2.1. Model development for shortcut design method

Generally the system proposed in this study (as referred to Fig. 1) can be divided into five major components namely, the fuel processor units (ATR and WGS reactor), hydrogen purification unit (membrane and PSA) and fuel cell stack.

2.2. Autothermal reformer (ATR)

Conceptually, coupling the partial oxidation, POX and steam reforming, SR (POX-SR) in a single reaction unit is called an auto-thermal reforming. ATR (stand-alone-reactor) could yield an energetically self-sufficient system for the production of H_2 [2], Heizel et al. (2003) [9,15–18] In other words, the process can be made thermally self-sustaining with no need for an external heat exchange. The ATR involves producing H_2 from methanol and steam while co-feeding with oxygen. The conversion of auto-thermal methanol steam to hydrogen combines two reactions namely, the highly endothermic steam reforming,

$$CH_3OH + H_2O \rightarrow CO_2 + 3H_2 = r_1 \quad (1)$$

and exothermic partial oxidation,

$$CH_3OH + 0.5O_2 \rightarrow CO_2 + 2H_2 + CO = r_2 \quad (2)$$

Both reactions produce hydrogen at different selectivity. Due to that, the selection of the feed ratio is very important in order to produce a high purity of hydrogen with necessary heat supply for the endothermic SR process by exothermic POX. Assuming the POX is a very fast reaction and the O_2 is supplied in limited condition, then the selectivity of H_2 over methanol and steam are given as below:

$$S_{H_2} = 3 - \frac{2M_0}{X_M}, \quad M_0 = \frac{C_{O_20}}{C_{M0}} \quad (3)$$

$$S_{H_2} = \left(\frac{M_S X_S}{X_M} + 2\right), \quad M_S = \frac{C_{S0}}{C_{M0}} \quad (4)$$

However, the selectivity will be based on the selectivity of oxygen because oxygen is supplied in limited amount while steam needs to be in excess in order to avoid reverse WGS reaction to occur. Assuming the pressure is constant in the ATR during the reaction and considering the varying-volume (or varying density), ε_V, the volume is linearly related to the conversion, or

$$V = \frac{F_{M0}}{\psi\rho(1-\varepsilon)} \int_0^X \frac{(1+\varepsilon_V X_M)^2\,dx}{k_1 C_{M0}^2 (1-X_M)(M_S - M_M) + k_2 C_{M0}^{1.5}(1+\varepsilon_V X_M)^{0.5}(1-X_M)(M_0 - X_M)^{0.5}} \quad (5)$$

where F_{M0} is the feed flow rate of methanol, ρ the catalyst density, ε the voidage of catalyst and ψ the dimensionless parameter for temperature. Eq. (5) can be solved graphically through integration or numerically using Simpson rule if the value of k_1 and k_2 are known.

2.3. Water gas shift reactor (WGS)

The other step of fuel processing is a water gas shift reaction (WGS). WGS is considered as secondary hydrogen producer and primary CO clean-up system. The carbon monoxide in the presence of steam will be converted to carbon dioxide and hydrogen. Although the typical industrial operating temperature for WGS reaction in fixed bed reactor ranges from 330 to 530 °C, however, this reaction is thermodynamically favoured at lower temperatures [8,18,19]

$$CO + H_2O \Leftrightarrow CO_2 + H_2 = r_3 \quad (6)$$

The selectivity of H_2 based on the CO in the feed stream to WGS reactor is given by

$$S_{H_2/CO} = \frac{C_{S0}X_{CO}}{C_{CO0}X_{CO}} = \frac{C_{S0}}{C_{CO0}} \quad (7)$$

From Eq. (7), it is observed that C_{S0} is proportional to hydrogen or carbon dioxide selectivity. Steam needs to be supplied in excess in order to yield more hydrogen by avoiding the reverse WGS from occur [18–20]. At constant pressure and isothermal condition, the volume of WGS reactor considering the recycle stream is predicted as below:

$$V = (R+1)\frac{F_{CO0}}{k_3\rho(1-\varepsilon)C_{CO0}^2} \int_{(R/(R+1))X_{CO,F}}^{X_{CO,F}} \times \frac{(1+\varepsilon_W X_{CO})^2\,dx}{(1-X_{CO})(M'_S - X_{CO})} \quad (8)$$

2.4. Tubular ceramic membrane (TCM)

The reformate from fuel processor units consists of hydrogen, carbon dioxide, carbon monoxide and residues of hydrocarbons. In this study, two separation units are introduced namely, the membrane unit and adsorber. Both membrane and adsorber will be operated in parallel to gain the product purity as 99.9% hydrogen and CO less than 10 ppm. Both porous and non porous (dense) inorganic membranes can be used as selective gas separation barriers. The separation factors of porous membranes are however much lower than those of Pd alloys, unless the pores are of molecular dimension. However due to hydrogen embrittlement, a phenomenon in which dissolved hydrogen tends to cause lattice expansion in the metal; eventually causing it to rupture on repeated pressure and temperature cycling, the new developments of porous membranes have given rise to many possibilities for catalytic membranes reactors [8], Hohlein et al. (2002).

The local permeation rate of component A over differential membrane area, dA_M, at any point in the stage is given as

$$y_1\,dn = \frac{K_1\,dA_M}{l_M}[x_1P_F - y_1P_P] \tag{9}$$

$$A_M = \int_{\text{retentate}}^{\text{feed}} \frac{l_M y_1\,dn}{P_{M,1}(x_1P_F - y_1P_P)} = \frac{l_M}{P_F K_1}\int_{X_{1F}}^{X_{1R}} \frac{y_1\,dn}{x_1 - ry_1} \tag{10}$$

Since the modelling is rated-based, the length of both modules could be expressed as the product of the height of a transfer unit (HTU) and the number of transfer unit (NTU).

Eq. (10) could be rewritten in the form of NTU and HTU by

$$L = \text{NTU} \times \text{HTU} = \frac{A_M}{n_T\pi D} = \frac{l_M}{P_F K_1 n_T \pi D}\int_{X_{1R}}^{X_{1F}} \frac{y_1\,dn}{x_1 - ry_1} \tag{11}$$

with n_T is defined as number of tubes, D the membrane diameter, l_m gives the membrane length, P_F the feed pressure and K_1 the permeability for component 1. The length of membrane in terms of HTU and NTU is given as below:

$$\text{where HTU} = \frac{l_M n_F}{P_F K_1 n_T \pi D_M} \tag{12}$$

and

$$\text{NTU} = \int_{X_{1R}}^{X_{1F}} \frac{y_1}{x_1 - ry_1}\left[\frac{1+(\alpha-1)x_1}{x_1(\alpha-1)(1-x_1)}(1-\theta)^2 \times \left[\left(\frac{x_1}{x_{1R}}\right)^{(1/(\alpha-1))}\left(\frac{1-x_{1R}}{1-x_1}\right)^{(\alpha/(\alpha-1))}\right]\right] dx \tag{13}$$

with x_1 and y_1 are defined as local retentate and permeate of component 1, respectively, at any point along the membrane. For local permeate, y_1, can be solved for each x_1 using equation:

$$\frac{y}{1-y} = \frac{\alpha^*(x-ry)}{(1-x)-r(1-y)} \tag{14}$$

where α^* is the ideal separation factor for multi-component gas in non-porous membrane and defined as (K_1/K_{mix}).

The mole fraction of component 1 in the final permeate based on crossflow module is obtained by

$$y_{1P} = x_{1R}{}^{(1/(1-\alpha))}\left(\frac{1-\theta}{\theta}\right)\left[(1-x_{1R})^{(\alpha/(\alpha-1))}\left(\frac{x_{1F}}{1-x_{1F}}\right)^{(\alpha/(\alpha-1))} - x_{1R}{}^{(\alpha/(\alpha-1))}\right] \tag{15}$$

where x_{1F} is the mole faction of component 1 in feed streams, $\theta = n_P/n_R$, $\alpha = (y_1/x_1)(x_2/y_2)$ = actual separation factor and while x_{1R} is the local rejection in the membrane unit.

The possible permeability for multi component gas is expressed as below:

$$K_{i,\text{mix}} = \frac{\varepsilon}{z\tau RT}\left[\frac{\bar{P}\,d_p^2}{8\mu_{i,\text{mix}}} + \left(\frac{1}{1/D_{i,\text{mix}} + 1/D_{kn}}\right)\right] + \frac{1}{\varepsilon}D_S\rho_M f \tag{16}$$

$\bar{P}$ is taken as operating pressure because the pressure in the pore is not measurable. Besides that $\mu_{i,\text{mix}}$, is defined as the average viscosity for the multi-component gases, where d_p the membrane pore diameter, ε_p the volume fraction in the pores, τ_{kn} the tortuosity, M the molecular weight of the gas and T the isothermal operating.

2.5. Pressure swing adsorber (PSA)

In this study, the PSA unit will be cooperated in parallel with membrane unit to reduce the CO concentration to less than 10 ppm before entering the fuel cell stack. Here we use a PSA, because it is found that PSA has a number of advantages in terms of product purity, product cost, operating cost, capital cost, product recovery, and high energy efficiency [21–23].

The adsorption of the component in a packed bed of adsorbent is given by [24]

$$-D_L\frac{\partial^2 c}{\partial z^2} + \frac{\partial(uc)}{\partial z} + \frac{\partial c}{\partial t} + \frac{(1-\varepsilon)}{\varepsilon}\frac{\partial \bar{q}}{\partial t} = 0 \tag{17}$$

where D_L is the axial dispersion coefficient, u the interstitial velocity, ε the bed porosity, q the concentration of the component in the adsorbed phase and c the concentration of the component in the gas phase in equilibrium with the adsorbed component. If axial dispersion is neglected ($D_L = 0$) and the velocity is constant, then the solution of Eq. (18) expressed as a breakthrough curve is given as

$$\frac{c}{c_F} \approx \frac{1}{2}\left[1 + \text{erf}\left(\sqrt{\tau} - \sqrt{\xi} + \frac{1}{8\sqrt{\tau}} + \frac{1}{8\sqrt{\xi}}\right)\right] \tag{18}$$

where c_F is the feed concentration of the component and

$$\xi \approx \frac{kKz}{u}\left(\frac{1-\varepsilon}{\varepsilon}\right) \tag{19}$$

$$\tau \approx k\left(t - \frac{z}{u}\right) \tag{20}$$

where k is the mass transfer coefficient and K the Henry constant. The length of the adsorber is estimated as the length of adsorbent fully saturated with the adsorbate in equilibrium with the component in the gas. The mass balance for this case gives

$$Q_F c_F t_{\text{ideal}} = \tfrac{1}{4}q_F(1-\varepsilon)L_b D_p^2 \tag{21}$$

The diameter of the bed, D_P is given as follows:

$$D_p = \left(\frac{4Q_F}{\varepsilon\pi u}\right)^{0.5} \tag{22}$$

A bed utilisation factor, $\tau/\xi \leq \tau_{ideal}/\xi$ and δ is defined by $\delta = t/t_{ideal}$ and by using this relationship between the ideal time and the ideal length, the ratio of Klinkenberg's dimensionless ideal time and Klinkenberg's dimensionless ideal length is given simply by

$$\frac{\tau}{\xi} = \left[\delta - \frac{\varepsilon}{(1-\varepsilon)K}\right] \tag{23}$$

Eq. (23) is solved simultaneously with Eq. (18) at c/c_F and various values of δ to get the actual curves of τ and ξ.

2.6. Fuel cell stack

PEMFC performance is limited by polarizations. A good understanding of the effect of design and operating conditions on the cell potential is required in order to reduce polarization. Major operating parameters include cell temperature, pressure, reactant stoichiometry, and gas stream composition. Generally PEMFC consists of three major components namely; anode, typically featuring a platinum or platinum-contain catalyst, a thin, solid polymeric sheet which acts as electrolyte, and a cathode, also platinum-catalyzed. The reactions in a hydrogen/oxygen fuel cell can be written as

$$\text{anode}: \quad 2H_2 \rightarrow 4e^- + 4H^+ \tag{24}$$

$$\text{cathode}: \quad 4e^- + 4H^+ + O_2 \rightarrow 2H_2O \tag{25}$$

$$\text{overall}: \quad 2H_2 + O_2 \rightarrow 2H_2O + \text{electricity} \tag{26}$$

2.7. The design of electrodes

The total area, A for the gas flow at any point on the electrode is given by

$$A = w\,dL \tag{27}$$

where w is the width for the gas distributor surface and dL is defined as differential element for length. Assuming the electrodes operates as a plug flow reactor, thus for reactant A

$$F_A = (F_A + dF_A) + (-r_A) \tag{28}$$

where F_A is the input of A (mol/time), (F_A+dF_A) the output of A (mol/time), X_A the conversion of A and rate of reaction A, r is obtained from:

$$r_A = \frac{i_n w\,dL}{nF} \tag{29}$$

for n = number of electron, i_n = current density and F = Faraday constant.

Substituting Eqs. (27)–(29), the simplified models of the gas composition is obtained as a function of axial distance:

The molar composition, C_A for each species in PEMFC electrodes is calculated from a set of given inlet composition gives

$$\frac{dC_A}{dL} = \frac{i_n w}{F_A nF} \quad \text{where } C_A = \frac{P_A y_A}{H_A} \text{ and } i_n = i_A y_A \tag{30}$$

with H_i = Henry constant, y_A = molar fraction of gas A and P_A = partial pressure of gas A.

From Eq. (30):

$$\frac{d[y_A P_A/H_A]}{dL} = \frac{i_A y_A w}{F_A nF} \tag{30a}$$

$$\frac{d[y_A]}{y_A} = \frac{H_A}{P_A}\frac{i_A w}{F_A nF}\int dL \tag{30b}$$

$$\ln(y_A) = \frac{H_A}{P_A}\frac{i_A w}{F_A nF}L$$

The gas composition for each species in PEMFC electrodes is calculated from a set of given inlet composition:

$$X_A = 1 - e^{[(H_A/P_A)(i_A w/F_A nF)L]} \tag{31}$$

The output voltage of the cell, considering thermodynamics, mass transport, kinetics, and ohmic resistance are described by [3,25–27]

$$V_{cell} = E_{nerst} - (\eta_{act} + \eta_{ohm} + \eta_{conc}) \tag{32}$$

At present, there exist a limited number of published PEMFC performance models, even more rare for the Ballard fuel cell [26].

Nerst equation for hydrogen/oxygen fuel cell is given as

$$E_{nerst} = 1.229 - (8.5\times10^{-4})(T - 298.15) + (4.308\times10^{-5})T(\ln p^*_{H_2} + \tfrac{1}{2}\ln p^*_{O_2}) \tag{33}$$

Activation polarization, η_{act}, is a result of the need to affect electron transfer and to break and form chemical bonds in the anode and cathode. The voltage loss due to activation is calculated by [25]

$$\eta_{act} = \xi_1 + \xi_2 T + \xi_3 T[\ln(c^*_{O_2})] + \xi_4 T[\ln(i)] \tag{34}$$

where the value of $c^*_{O_2}$ is defined as the water effluent from the outlet of cathode

$$\xi_1 = -\frac{\Delta G_{ec}}{2F} - \frac{\Delta G_e}{\alpha_c nF},$$

$$\xi_2 = \frac{R}{\alpha_c nF}\ln\left[nFAk^0_c(c^*_{H_2})^{1-\alpha_c}c^*_{H_2O}\right] + \frac{R}{2F}\ln\left[4FAk^0_a c^*_{H_2}\right],$$

$$\xi_3 = \frac{R(1-\alpha_c)}{\alpha_c nF}, \qquad \xi_4 = -\left(\frac{R}{2F} + \frac{R}{\alpha_c nF}\right)$$

Ohmic polarization, η_{ohm}, is caused by electrical resistance losses in the cell. Electrical resistance is found in the electrodes, the membrane (ionic), the fixtures that connect the membrane-electrode assemblies (MEAs), and the interfaces

between each component. The total ohmic polarization is defined as (Bashuk and Xianguo, 2000) [33]:

$$\eta_{ohm} = \eta^{e}_{ohm} + \eta^{p}_{ohm} + \eta^{m}_{ohm} = 2iwL(\xi_5 + \xi_6) + \xi_7 \quad (35)$$

where

$$\xi_5 = \frac{\rho^{eff}_{R,e}}{8 n_g \delta_e L}(w_c + w_s) \quad \text{and} \quad \rho^{eff}_{R,e} = \frac{\rho_{R,e}}{(1-\phi_e)^{3/2}},$$

$$\xi_6 = \frac{\rho_{R,p}}{L}\left(\frac{h_p}{W} + \frac{h_c}{W - n_g w_c}\right),$$

$$\xi_7 = \delta_m \frac{(I_\delta / K_m) + (F K_p C_{H^+} \Delta P_{a-c} / K_m \mu_{H_2O} \delta_m)}{1 + F^2 K_E C^2_{H^+} / K_m \mu_{H_2O}}$$

However, the ohmic polarization can be reduced by using components that have a high electrical conductivity and reducing the thickness of the membrane layer, where the actual values of η^{e}_{ohm} and η^{m}_{ohm} should not be significant in comparison to η^{p}_{ohm} and can be assumed to be insignificant [4,23].

Eq. (36) is an empirical approach to capture the smooth drop-off of the polarization curves at elevated current densities [28]. The parameters m and n are of empirical nature and assumed as 0.000312 and 0.008, respectively. Besides that Table 1 gives the value of the polarization parameters

$$\eta_{conc} = m\, e^{ni} \quad (36)$$

2.8. Material balance and heat balance

Fig. 2 presents the flow chart diagram for overall material balance of the system. Basically there are 15 numbers of process streams in the system. The following paragraph will develop the equations for the material balance in every unit.

Table 1
The values of the polarization parameters

Parameter	Values	Typical
E_{nerst}	1.182	0.953
η_{act}		
ξ_1	-0.948	9.8×10^{-3}
ξ_2	3.93×10^{-3}	9.8×10^{-3}
ξ_3	6.8×10^{-5}	9.8×10^{-3}
ξ_4	-1.97×10^{-4}	9.8×10^{-3}
η_{ohm}		
ξ_5	3.30×10^{-3}	0.35
ξ_6	-7.55×10^{-6}	0.35
ξ_7	-8.60×10^{-5}	0.35

The overall reaction involved in ATR is given by

$$CH_3OH + 0.5H_2O + 0.25O_2 \rightarrow 2.5H_2 + CO_2 + (CO) \quad (37)$$

From Fig. 2, the flow rate of reactant is defined as

$$F_{M,1} = F_{M0} \quad (38)$$

$$F_{H_2O,2} = F_{S0} = \left(\frac{S}{C}\right) F_{M0} \quad (39)$$

$$F_{O_2,3} = F_{O_2 0}\left(\frac{O_2}{C}\right) F_{M0} \quad (40)$$

Let n_1 = degree of the reaction and α_i = stoichiometric. It is defined as negative for feed reactant and positive for product

$$n_1 = \frac{X_M F_{M,1}}{-\alpha_M} \quad (41)$$

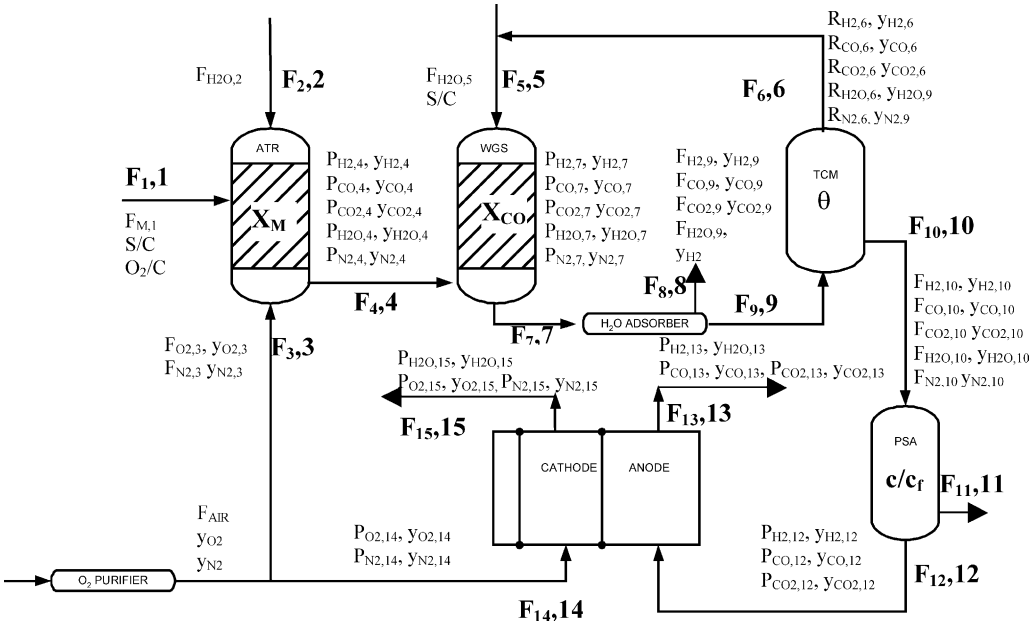

Fig. 2. Flowchart shows the material balance of the system.

The product gas for ATR is given by

- The mass balance for H_2:

$$P_{H_2,4} = \alpha_{H_2} n_1 = S_H X_M F_{M0} \quad (42)$$

- The mass balance for CO_2:

$$P_{CO_2,4} = \alpha_{CO_2} n_1 \quad (43)$$

- The mass balance for CO:

$$P_{CO,4} = \alpha_{CO} n_1 \quad (44)$$

- The mass balance for steam:

$$P_{H_2O,4} = F_{H_2O} + \alpha_{H_2O} n_1 \quad (45)$$

- The mass balance for methanol:

$$P_{M,4} = F_{M0} + \alpha_M n_1 \quad (46)$$

- The mass balance for N_2:

$$P_{N_2,4} = y_{N_2,3} F_{O_2,3} \quad (47)$$

The product from ATR will enter the WGS reactor. WGS reaction converts carbon monoxide in the presence of steam to produce carbon dioxide and hydrogen. Basically for WGS reaction, the equation is given as below:

$$CO + H_2O \Leftrightarrow CO_2 + H_2 \quad (48)$$

Let

$$n_2 = \frac{X_{CO} F_{CO,4}}{-\alpha_{CO}} \quad (49)$$

The mass balances of product stream from WGS reactor are given as below:

- The mass balance for H_2:

$$P_{H_2,7} = (P_{H_2,4} + R_{H_2,6}) + \alpha_{H_2} n_2 \quad (50)$$

- The mass balance for CO_2:

$$P_{CO_2,7} = (P_{CO_2,4} + R_{CO_2,6}) + \alpha_{CO_2} n_2 \quad (51)$$

- The mass balance for CO:

$$P_{CO,7} = (P_{CO,4} + R_{CO,6}) + \alpha_{CO} n_2 \quad (52)$$

- The mass balance for steam:

$$P_{H_2O,7} = \frac{S}{C} P_{CO,4} + \alpha_{H_2O} n_2 \quad (53)$$

- From Fig. 2,

$$F_5 = \frac{S}{C} P_{CO,4} - (P_{H_2O,4} + F_8 + R_{H_2O,6}) \quad (54)$$

From WGS reactor, the product will pass through a water adsorber unit in order to remove the excess steam in the stream before entering the membrane unit. This is required because excess of water in the membrane could reduce the performance of the membrane. The material balance around the water adsorber is given as

$$F_9 = (1 - y_{H_20,7}) F_7 \quad (55)$$

F_8 is the water product from the adsorber and will be recycled back to the WGS reactor. $F_{9,}$ is the inlet stream to the membrane unit. In Fig. 3, the retentate stream for membrane is defined as $R_{i,6}$. This stream will be recycled back to WGS reactor to convert the CO to hydrogen with the presence of excess steam while the permeate stream is defined as, F_{10}. The overall material balance for membrane is given by

$$F_9 = F_6(1 - \theta) + F_{10}\theta \quad (56)$$

From the membrane unit, the permeate will enter the pressure swing adsorber for further CO removal.

- The material balance for H_2:

$$F_{10} y_{H_2,10} = F_{11} y_{H_2,11} + F_{12} y_{H_2,12} \quad (57)$$

- The material balance for CO:

$$F_{10} y_{CO,10} = F_{11} y_{CO,11} + F_{12} y_{CO,12} \quad (58)$$

Finally, after the adsorber unit, the fuel cell will enter the anode side of the fuel cell stack.Fuel cell stack are formed of

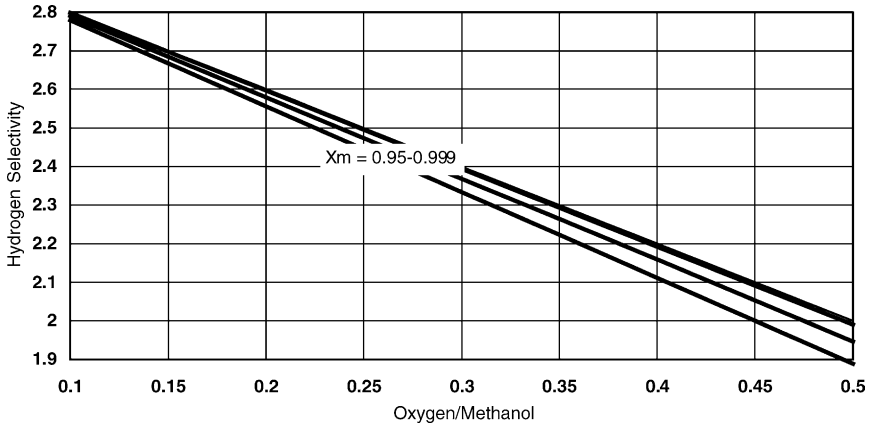

Fig. 3. The hydrogen selectivity for different oxygen/methanol ratio.

a perfluosulfonic membrane as electrolyte coupled with two electrodes (anode and cathode) built utilizing a substrate of carbon-PTE coated with platinum as electrocatalyst. Oxygen is fed to the cathodic compartment while hydrogen is fed to the anodic one and the electrolyte performs both the function of transferring H^+ from the anode to the cathode and reactant separation. The overall material balances for fuel cell stack are below assuming other components like, N_2, CO and CO_2 are constant.

- For hydrogen:

$$P_{H_2,13} = P_{H_2,12} - 2\left(\frac{i_a A}{P_{H_2,12} 4F}\right) \tag{59}$$

- For oxygen:

$$P_{O_2,13} = P_{O_2,12} - \frac{i_c A}{P_{H_2,12} 2F} \tag{60}$$

- For water:

$$P_{H_2O,15} = 2\left(\frac{i_a A}{P_{H_2,12} 4F}\right) + k_a(y_{H_2O} - y^*_{H_2O}) + k_c(y_{H_2O} - y^*_{H_2O}) \tag{61}$$

where k_a and k_c are defined as the mass transfer coefficient.

2.9. Heat balance

Heat management is one of the important problems in both low-temperature and high temperature fuel cells. Fuel cell models can be built-up upon the conventional heat balance equation, but further consideration of electrochemical reaction and its consequences should be taken into account at the same time [29]. In the foregoing section the energy balance of the system is described. From the energy balance, the net and gross efficiency of the system can be estimated.

ATR is a thermally neutral process. ATR is combination of steam reforming and partial oxidation process. Steam reforming process is highly endothermic while partial oxidation is a exothermic process and this results to adiabatic or slightly exothermic process for ATR. At the steady state, the net thermal energy balance for the reformer can be calculated by the following relations:

$$Q_{ATR} = \sum_P n_e[h_f^0 + \Delta\bar{h}] - \sum_r n_i[h_f^0 + \Delta\bar{h}] \tag{62}$$

Water gas shift reaction is an isothermal process [19] and it is normally operated at 200–250 °C [18]. The energy balance across the WGS reactor is referred to equation:

$$Q_{ATR} = \sum_P n_e[h_f^0 + \Delta\bar{h}] - \sum_r n_i[h_f^0 + \Delta\bar{h}] \tag{63}$$

The TCM and PSM are operated at adiabatic condition. From PSA, the stream will enter the fuel cell stack. For the purpose of energy balance, it was assumed that the anode and cathode gas would enter and leave the stack at a temperature of 70 °C. The stack was thermally insulated, therefore heat balance to the surroundings was assumed to be negligible. The overall fuel cell reaction is a formation of water from hydrogen and oxygen, producing electricity and heat. The relation of cell reaction and formation of water from H_2 and O_2 is given by

$$Q_{anode} = \sum_{H_2} (C_{p,i} y_i) T_{a,out} - \sum_{H_2} (C_{p,i} y_i) T_{a,in} \tag{64}$$

The energy balance for the fuel cell stack is given by

$$Q_{cooling\,water} = Q_{cell} - (Q_{cathode} + Q_{anode} + Q_{loss}) \tag{65}$$

The energy conversion efficiency of fuel cell is higher than of combustion engines or boilers. Yet a significant amount of heat is released during the cell reaction. Thus, the heat flux from the cell reaction depends on the hydrogen fraction consumed by the cell reaction and on the current. The heat flux is expressed by using enthalpy of the reaction as follows:

$$Q_{cell} = (\Delta H_{f,H_2O}) r_{H_2} - Q_E \tag{66}$$

where Q_E is the power output of the stack.

$$Q_{cell} = \left[\sum_{H_2O} n_e[h_f^0 + \Delta\bar{h}] - \sum_{r,i} n_i[h_f^0 + \Delta\bar{h}]\right] \frac{i}{2F} - iV_{cell}, \quad i = H_2, O_2 \tag{67}$$

The heat flux by each gas that comes in and goes out of the stack is expressed by

$$Q_{cathode} = \sum_{H_2O,O_2} (C_{p,i} y_i) T_{c,out} - \sum_{O_2} (C_{p,i} y_i) T_{c,in},$$

$$Q_{anode} = \sum_{H_2} (C_{p,i} Y_i) T_{a,out} - \sum_{H_2} (C_{p,i} Y_i) T_{a,in} \tag{68}$$

To evaluate the thermal radiation from the stack, Q_{loss} three terms were taken into account [30]:

$$Q_{loss} = Q_{stack} + Q_{side} + Q_{rod} \tag{69}$$

where Q_{stack} = heat loss from the stack such as compression plate, Q_{side} = stack side thermal insulation wall, and Q_{rod} = stack compressions rod

$$Q_{stack} = \sum (A_j K_j (T_{i-out} - T_{i-in})) \tag{70}$$

$$Q_{side} = \sum \left(\frac{A_j \lambda_T}{\delta_R (T_{i-out} - T_{i-in})}\right) \tag{71}$$

$$Q_{rod} = \sum \left(\frac{\pi}{4d^2} \frac{\lambda_R}{\delta_R (T_{i-out} - T_{i-in})}\right) \tag{72}$$

where $i = A_{in}$, A_{out}, C_{in}, C_{out}, and j = top, bottom, A the effective heat transfer area, δ the thickness, λ the heat conductivity, d the diameter of the compression rod and K the overall coefficient of heat transfer and is given by

$$K = \frac{1}{\delta_T/\lambda_T n_T + \delta_F/\lambda_F n_F + \delta_P \lambda_P} \tag{73}$$

where *n* is the number of part, and subscript is for the compression plate, T for the thermal insulator, F for the felt, and R for the compression rod.

3. Results and discussion

3.1. Hydrogen selectivity for fuel source

The primary fuel source to the ATR system is methanol, which is fed together with steam and oxygen. The ratio of the three reactants can vary and are often chosen such that the overall reaction is thermal–neutral or only modestly exothermic. The ratio of oxygen and steam over methanol are illustrated by Figs. 3 and 4. The ratio of O_2:MeOH is found to be between 0.20 and 0.25 for optimum methanol usage and to ensure the overall reaction are thermally neutral in terms of energy usage.

The hydrogen selectivity at this point is around 2.5–2.6 for complete conversion of methanol, while for steam:MeOH, the selectivity is obtained about 0.45–0.5 to yield the hydrogen selectivity of 2.5–2.6 for optimum methanol feed as shown in Fig. 3. With that, the ratio of MeOH:O_2 is taken as 1:0.25, however the steam is supplied in excess, therefore the ratio of steam:MeOH is taken and 1:1.3, respectively. The calculated hydrogen selectivity is used to determine the amount of methanol needed to produce the required amount of hydrogen.

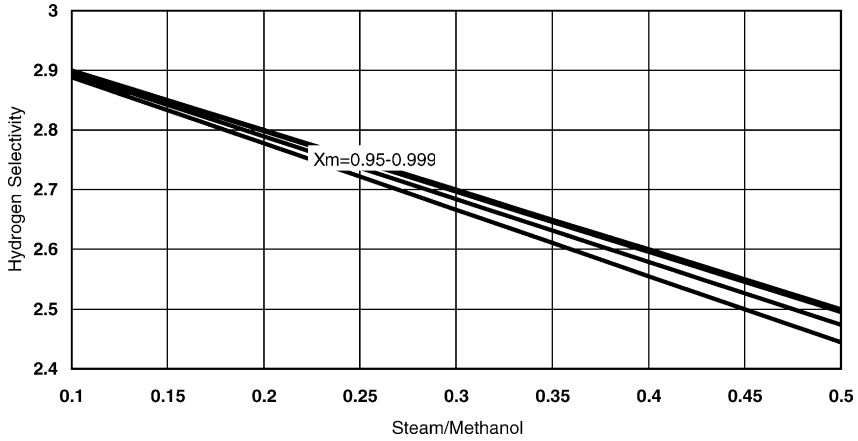

Fig. 4. The hydrogen selectivity for different steam/methanol ratio.

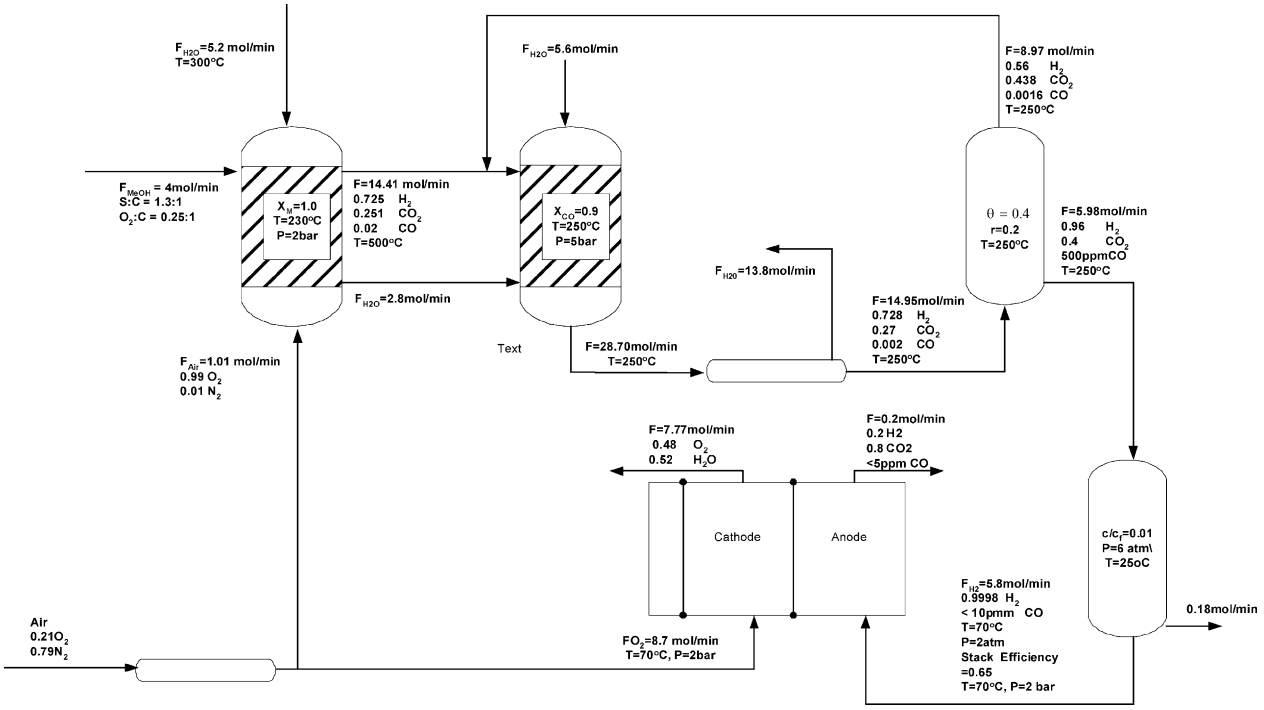

Fig. 5. Results of material balance and design parameters.

3.2. Material balance

Taking the hydrogen consumption in the fuel cell stack as 1000 L/h of hydrogen for a power output of 1 kW_e, the total hydrogen required at the stack for a power output of 5 kW is calculated as 3.74 mol/min (0.17 m^3/min). As for a base case, feed flow rate of methanol, F_{MeOH} is taken as 4 mol/min (0.1 m^3/min). Fig. 5 summarized the overall material balance in mole percentage.

From the overall mass balance, the product from ATR is determined as—H_2: 73%, CO: 2%, and CO_2: 25%. In the WGS reactor, it is observed that the hydrogen recovery after the WGS is only about 0.3–0.6% but the mole fraction of CO is found to decrease from 2% to about 0.2%. Although this is a very small drop but it is very significant in the PEMFCs system because the concentration of CO reduces from 20,000 ppm (after the reformer) to less than 2000 ppm (after the WGS), assuming no reverse WGS reaction occurs. However, if CO is being produced thermodynamically by the reverse water gas shift reaction due to the excess steam, it will only be in the range of 20–50 ppm [19]. As such results, it denied the acquisition [15,18], that the WGS was not needed in the fuel processor as one of the CO clean up system. Although the main problem in WGS process is the low temperature for catalyst activity and expected to be the largest component in the system but this paper proves that WGS reaction is very important in PEMFC unit as secondary hydrogen source and primary CO clean-up unit. Furthermore, the conceptual design proves that pressure can be used as a control parameter to reduce the size of the WGS reactor. CO is further reduced to 500 and less than 10 ppm after the TCM and PSA. Finally, the hydrogen at the inlet side of anode is expected to be at 99.98%. Beside that, Fig. 6 presents a summary of the heat balance across the system as calculated by using the method explained in previous section.

Neglecting the thermal radiation from the stack, Q_{loss}, the waste heat generated in the fuel cell stack is calculated as 1.4 kW.

3.3. Fuel cell system efficiencies

The net efficiency of fuel cell power plant can be calculated based on the stack electrochemical efficiency of 65%, and the power conditioner efficiency is suggested to be 90% based on fuel processor and parasitic load [4]. The power conditioner efficiency includes both rectifier and converter [31]. The parasitic load energy includes all of the electrical power that will be required to run any pumps and compressor in the system. The parasitic load for PNGV automobile with power output for 4–6 kW is estimated as 400 W using mathematical models [32]. The base operating conditions for the system are shown in Table 2.

Table 2
Fuel cell/fuel processing operating condition for base-case scenario

Parameter	Value
Reformer temperature	250 °C
Reformer pressure	2 bar
Feed flow rate of MeOH	4 mol/min
Steam/MeOH	1.3:1
O_2/MeOH	0.25:1
WGS temperature	250 °C
WGS pressure	5 bar
Steam:CO	30:1
TC membrane temperature	250 °C
TC membrane H_2 outlet temperature	1 bar
PSA temperature	80 °C
PSA pressure	6 bar
Stack pressure	2 bar
Stack temperature	70 °C
H_2/O_2 ratio in the stack	1.5
Fuel cell current density	900 mA/cm^2

The cell efficiency is defined as [5]

$$\eta = \frac{V_{cell}}{V_{ref}} \tag{74}$$

For hydrogen: $V_{ref} = 1.25$ V; while for methanol, $V_{ref} = 1.08$ V. The portion of H_2 for ATR and WGS can be calculated using the higher heating value of H_2, HHV

$$(H_2)_{ATR} = \frac{Q^0_{rf}}{HHV} = 0.11 \text{ kmol of } H_2 \tag{75}$$

$$(H_2)_{WGS} = \frac{Q_{WGS}}{HHV} = 0.17 \tag{76}$$

$$\varepsilon_{gross} = \varepsilon_{fuel\ cell}\varepsilon_{power\ conditioner}\varepsilon_{ATR}\varepsilon_{WGS} = \frac{(0.65)(0.96)(2.5-0.11)(1-0.17)}{2.5} = 49.5\% \tag{77}$$

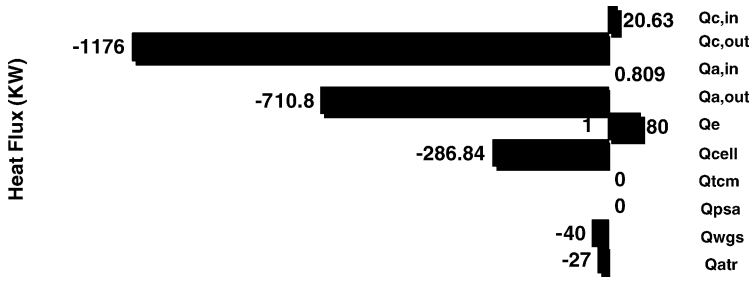

Fig. 6. Results of overall heat balance across the system.

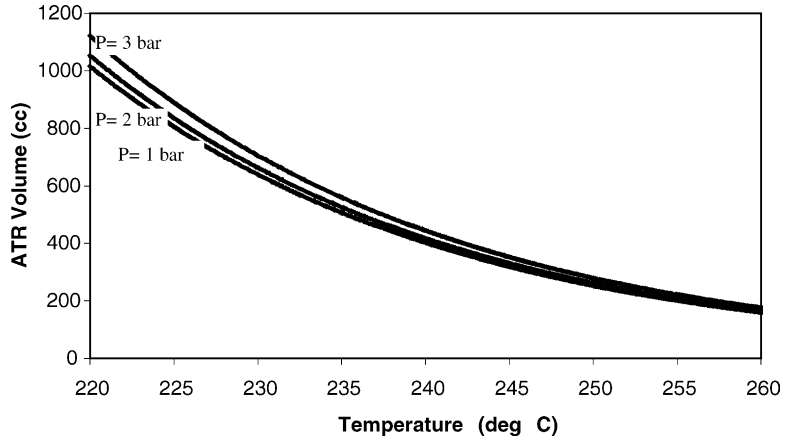

Fig. 7. Shows the volume for ATR at different temperature and pressure.

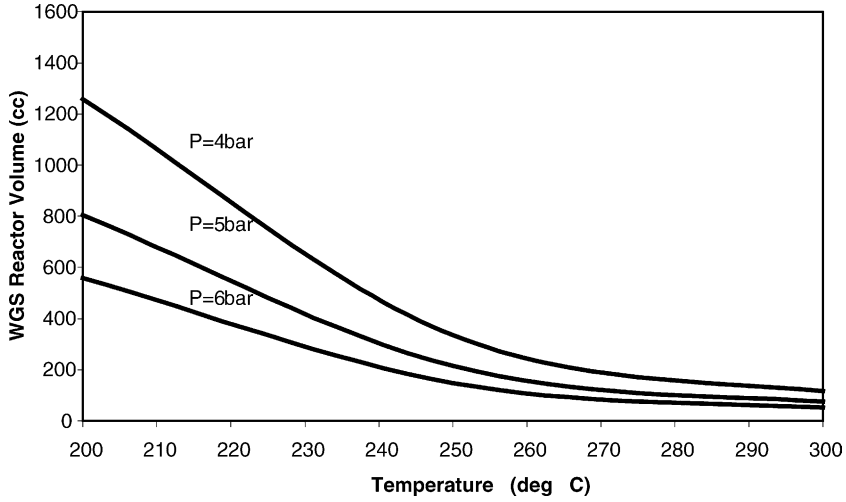

Fig. 8. Shows the volume for WGS reactor at different temperature and pressure.

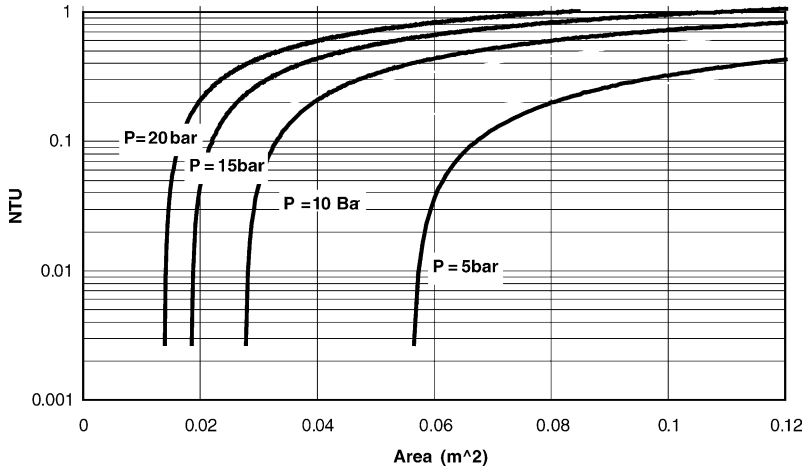

Fig. 9. Results of the NTU and A_M for ceramic membrane for different operating pressure.

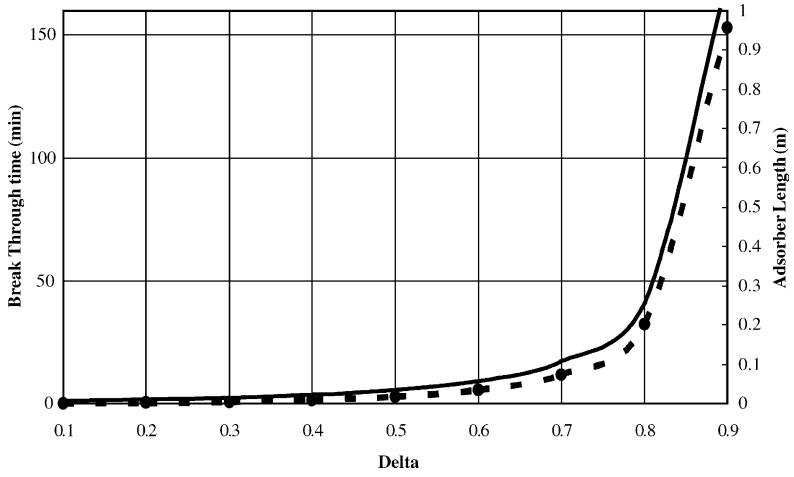

Fig. 10. Plots show the break through time and the PSA length.

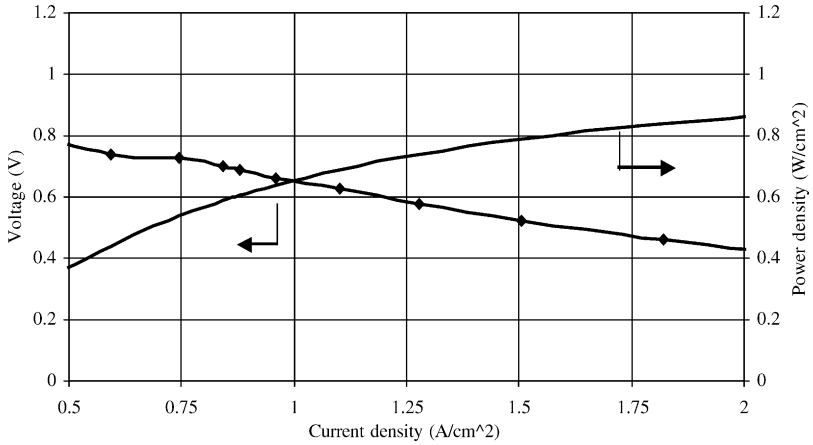

Fig. 11. The characterization of fuel cell stack for this study.

$$\varepsilon_{\text{net}} = \varepsilon_{\text{gross}}\varepsilon_{\text{parasitic load}} \quad (78)$$

The base-case simulation was compared to a variety of operating condition. The operating temperature and pressure for ATR and WGS reactor were varied between 220 and 260 °C and from 1 to 5 bar, while the ratio of O_2:MeOH and steam:CO were maintained at 1:4 and 1:30, respectively (refer to Figs. 7 and 8). The pressure for membrane was varied from 5 to 20 bar (refer to Fig. 9), and the solution of bed length was then expressed as a function of the bed utilisation factor, δ for adsorber (refer to Fig. 10). Finally Fig. 11 presents the voltage, current density and power density for the fuel cell stack in this study. As the objective of this study is to conceptually design a 5 kW PEMFC via simulation, hence Table 3 presents the principal variables and the output condition for the base case.

From the base simulation, the parasitic load was over 8% of the total power produced. The gross efficiency is calculated as 49.5% while the net efficiency is estimated as 45.5%. Note that the heat losses from the heat exchangers are neglected in this study. The TCM and PSA are presumably operated at adiabatic condition.

Table 3
output conditions for base-case simulation

Parameter	Value
ATR exit: dry mol fraction of H_2	72.2%
ATR exit: dry mol fraction of CO	2%
Methanol flow to ATR	5.76 kg/h
Volume of ATR	250 cm^3
WGS exit: dry mol fraction of H_2	72.8%
WGS exit: dry mol fraction of CO	0.2% ppm
Volume of WGS	400 cm^3
TC membrane recovery of H_2	95% (at $\theta = 0.4$)
Membrane: dry mol of CO	0.05%
Size of membrane	10 cm × 25 cm
PSA purification	99.98% (at $c/c_f = 0.01$)
CO concentration before entering stack	<10 ppm
Size of PSA	0.22 cm × 0.25 cm
Voltage for single cell	0.7 V
Active surface area	247 cm^2 × 30 number of cell
Power conditioner efficiency	90%
Fuel cell efficiency	65%
Fuel processor efficiency	80%
Parasitic load	0.4 kW
Net efficiency	45.5%
Electrical power produced	5.5 kW/dc

4. Conclusion

A simulation based on shortcut design methods was used to design a PEM fuel cell. The first part of this paper expresses the short-cut design methods for ATR, WGS, Membrane, PSA fuel cell stack in the PEMFC system based on the design parameters for each units. It also shows the expression for actual rate of reaction in ATR and WGS, selectivity of methanol over steam and water for feed source, and the reactor design considering variations in volume that are always neglected by most of the researchers. From most of the previous studies, the design of the ATR is solely based on the steam reforming reaction by assuming the partial oxidation happens very fast. In this paper, however, the rate of reaction is derived based on both reactions by considering the varying of the volume expansion. For membrane unit, the expression of length and surface area is simplified in terms of NTU and HTU. The term NTU relatively describes the degree of separation relative, and HTU describes the physical and mechanical property of the selected membrane. Besides that, as a PSA process is quite complicated and there are many parameters to be decided, here we simplify the design of the PSA by using the Klinkenberg solution of the breakthrough curve for a linear driving force mass transfer and a linear equilibrium isotherm, and a relationship between the dimensionless time, τ, and the dimensionless bed length, ξ, which are the function of the bed utilisation parameter, δ. Daud bed utilisation factor derived by one of the authors is also introduced in this paper as bed utilisation parameter. Finally, a mathematical model of PEM fuel cell stack is also presented by taking into consideration all the polarization factor, current density and mole fraction of gases and polarization behaviour along the gas surface area.

Hydrogen was produced from methanol and water by auto-thermal reformer. The CO produced from ATR (20,000 ppm) later was reduced to less than 2000 ppm by WGS. After that the stream enters the TCM and PSA for the purpose of H_2 purification. Finally the flow enters the stack as 99.9% of hydrogen and 5 ppm of CO. A systematic evaluation for the performance of a fuel cell power plant using methanol as fuel is undertaken by obtaining the power plant efficiency. The results indicate that the gross power plant efficiency is 49.5%. This gross power efficiency includes the fuel cell, power conditioner and fuel processor efficiency only. Upon considering the parasitic load as 8%, the net power plant efficiency reduces to 45.5%.

Acknowledgements

The authors gratefully acknowledge the financial support given for this work by the Malaysian Ministry of Science, Technology and Environment (MOSTE) under the Intensification Research in Priority Areas (IRPA) by Grant No.: IRPA 02-02-02-0001-PR0023 11-06.

References

[1] J. Han, I.S. Kim, K.S. Choi, Purifier-integrated methanol reformer for fuel cell vehicles, J. Power Sour. 86 (2000) 223–227.
[2] N. Edvards, S.R. Ellis, J.C. Frost, S.E. Golunski, A.N.J. Van Keulen, N.G. Linderwald, J.G. Reinkingh, On-board hydrogen generation for transport application: the Hotspot methanol processor, J. Power Sour. 71 (1998) 123–128.
[3] M.D. Francesco, E. Arato, Start-up analysis for automotive PEMFC systems, J. Power Sour. 108 (1/2) (2002) 41–52.
[4] J.C. Amplett, R.F. Mann, B.A. Pepply, P.R. Roberge, A. Rodrigues, J.P. Salvador, Simulation of a 250 kW diesel fuel processor/PEM fuel cell system, J. Power Sour. 71 (1998) 179–181.
[5] C. Bernay, M. Marchand, M. Cassir, Prospects of different fuel cell technologies for vehicle application, J. Power Sour. 108 (1/2) (2002) 139–152.
[6] D. Chu, R. Jiang, Performance of polymer electrolyte membrane fuel cell (PEMFC) stacks, J. Power Sour. 83 (1999) 128–133.
[7] D. Chu, R. Jiang, K. Gardner, R. Jacobs, J. Schmidt, T. Quakenbush, J. Stephens, PEMFCs for communication application, J. Power Sour. 96 (2001) 174–178.
[8] D.R. Palo, J.D. Holladay, R.T. Rozimiarek, C.E.G. Leong, J. Wang, J. Hu, Y.H. Chin, R.A. Dagle, E.G. Baker, Development of a soldier-potable fuel cell power system, J. Power Sour. 108 (2002) 28–34.
[9] B. Höhlein, M. Boe, J. Bøgild-Hansen, P. Bröckerhoff, G. Colsman, B. Emonts, R. Menzer, E. Riedel, Hydrogen from methanol for fuel cells in mobile systems: development of a compact reformer, J. Power Sour. 61 (1–2) (1996) 143–147.
[10] A. Heinzel, C. Hebling, M. Müller, M. Zedda, C. Müller, A. Henzel, Fuel cells for low power applications, J. Power Sour. 105 (2) (2002) 250–255.
[11] J.P. Meyers, H.L. Maynard, Design considerations for miniaturized PEM fuel cells, J. Power Sour. (2002) 1–14.
[12] C.E.B. Bird, Fuel cell commercialization issues for light duty vehicle applications, J. Power Sour. 61 (1996) 33–48.
[13] J. Cunha, J.L.T. Azevedo, Modeling the integration of a compact plate steam reformer in a fuel cell system, J. Power Sour. 86 (2000) 515–522.
[14] K.L. Hey, J. Roes, R. Wolters, CO_2—scrubbing and methanation as purification system for PEFC, J. Power Sour. 86 (1/2) (2000) 556–561.
[15] L. Ma, D.L. Trimm, C. Jiang, The design and testing of an autothermal reactor for the conversion of light hydrocarons to hydrogen. I. The kinetics of the catalyst oxidation of light hydrocarbons, Appl. Catal. A: Gen. 138 (1996) 275–283.
[16] R. Jiang, D. Chu, Voltage–time behavior of a polymer electrolyte membrane fuel cell stack at constant current discharge, J. Power Sour. 92 (2001) 193–198.
[17] P. Mizsey, E. Newson, T.H. Truong, P. Hottinger, The kinetic of methanol decomposition: apart of autothermal partial oxidation to produce hydrogen foe fuel cells, Appl. Catal. A: Gen. 213 (2001) 233–237.
[18] J.M. Zalc, D.G. Loffler, Fuel Processing for PEM fuel cells: transport and kinetics issues of system design, J. Power Sour. 4869 (2002) 1–7.
[19] A.Y. Tonkovich, J.L. Zilka, M.J. Lampunt, Y. Wang, R.S. Wegeng, Micro channel reactors for fuel cell processing application. I. Water gas shift reactor, Chem. Eng. Sci. 54 (1999) 2947–2951.
[20] E.D. Doss, R. Kumar, R.K. Ahluwalia, M. Krumpelt, Fuel processor for automotive fuel cell systems: a parametric analysis, J. Power Sour. 102 (2001) 1–15.
[21] S.E. Iyuke, W.R.W. Daud, A.B. Mohamad, A.A.H. Kadhum, Z. Fisal, A.M. Shariff, Application of Sn-activated carbon in pressure swing adsorption for purification on H_2, J. Chem. Eng. Sci. 55 (2000) 4745–4755.
[22] R. Rajasree, A.S. Moharir, Simulation based synthesis, J. Comput. Chem. Eng. 24 (11) (2000) 2493–2505.

[23] S. Jain, A.S. Moharir, P. Li, G. Wozny, Heuristic design of pressure swing adsorption: a preliminary study, J. Separat. Purif. Technol. 33 (2003) 25–43.
[24] W.R.W. Daud, A short-cut design method for adsorber used in gas dryers and dehumidifiers, in: Proceeding of the SOMCHE, 2001.
[25] A. Rowe, X. Li, Mathematical modeling of proton exchange membrane fuel cells, J. Power Sour. 102 (2001) 82–96.
[26] M.W. Fowler, R.F. Mann, J.C. Amphlett, B.A. Peppley, P.R. Roberge, Incorporation of voltage degradation into a generalized steady state electrochemical model for a PEM fuel cell, J. Power Sour. 106 (2002) 274–283.
[27] J. Larminie, A. Dicks, Fuel Cell System Explained, Wiley, 2001.
[28] R.F. Mann, J.C. Amphlett, M.A.I. Hooper, H.M. Jensen, B.A. Peppley, P.R. Roberge, Development and application of a generalised steady-state electrochemical model for a PEM fuel cell, J. Power Sour. 86 (1–2s) (2000) 173–180.
[29] J.H. Koh, H.K. Seo, Y.S. Yoo, H.C. Lim, Consideration of numerical simulation parameters and heat transfer models for a molten carbonate fuel cell stack, Chem. Eng. J. 87 (2002) 367–379.
[30] Y. Miyake, N. Nakanishi, T. Nakajima, Y. Itoh, T. Saito, A. Saiai, H. Yanaru, A study of heat and material balances in an internal-reforming molten carbonate fuel cell, J. Power Sour. 56 (1995) 11–17.
[31] C. Wallmark, P. Alvfors, Design of Stationary PEFC system configurations to meet heat and power demands, J. Power Sour. 106 (2002) 83–92.
[32] S.H. Lee, J. Han, K.Y. Lee, Development of 10 kW_e preferential oxidation system for fuel cell, J. Power Sour. 109 (2002) 356–364.
[33] J.J. Baschuk, L. Xianguo, Modelling of polymer electrolyte membrane fuel cells with variable degrees of water flooding, J. Power Sour. 86 (2000) 181–196.